Japanese Journal of Applied Physics **53**, 08NM01 (2014) **REGULAR PAPER**
http://dx.doi.org/10.7567/JJAP.53.08NM01

Exchange bias in $BiFeO_3/La_{0.67}Sr_{0.33}MnO_3$ bilayers

Qingyu Xu[1,2,3*], Yan Sheng[1], Xiaobo Xue[3,4], Xueyong Yuan[1], Zheng Wen[5], and Jun Du[3,4*]

[1]*Department of Physics, Southeast University, Nanjing 211189, China*
[2]*Key Laboratory of MEMS of the Ministry of Education, Southeast University, Nanjing 210096, China*
[3]*National Laboratory of Solid State Microstructures, Nanjing University, Nanjing 210093, China*
[4]*Department of Physics, Nanjing University, Nanjing 210093, China*
[5]*Department of Materials Science and Engineering, Nanjing University, Nanjing 210008, China*
E-mail: xuqingyu@seu.edu.cn; jdu@nju.edu.cn

Received December 29, 2013; accepted March 14, 2014; published online July 10, 2014

The exchange bias in $BiFeO_3/La_{0.67}Sr_{0.33}MnO_3$ (BFO/LSMO) bilayers has been investigated. Exchange bias field with blocking temperature of about 150 K and enhanced coercivity at room temperature has been observed in (001) BFO/LSMO bilayers. The blocking temperature coincides well with the emerging temperature of the vertical magnetization shift due to the blocking of the possible interfacial spin glass. Only enhanced coercivity without exchange bias field down to 10 K has been observed in (111) BFO/LSMO bilayers. The piezoelectric force microscopy images show that the domain size of (111) BFO is 2 orders larger than that of the (001) BFO, indicating the much higher domain wall density in (001) BFO. Our results demonstrate that the exchange coupling with interfacial spin glass at the domain walls contributes to the exchange bias field with blocking temperature of about 150 K, while the exchange coupling with the domains contributes to the enhanced coercivity up to room temperature.
© 2014 The Japan Society of Applied Physics

1. Introduction

With multiferroic materials integrated into spintronics devices, the spins might be manipulated by the electric field, leading to the development of the next generation of low power-consumption, high-speed information technologies.[1)] Much attention has been paid on $BiFeO_3$ (BFO) due to that it is possibly the only room temperature (RT) multiferroic material with ferroelectric Curie temperature ($T_{C\text{-}FE} \sim 1100$ K) and antiferromagnetic (AFM) Neel temperature ($T_N \sim 640$ K).[2)] The coupling between the AFM and ferroelectric orderings has been confirmed experimentally by the observation of coupled AFM and ferroelectric domains.[3)] The most plausible application in spintronics for BFO is the AFM pinning layer,[4)] and exchange bias has been reported on BFO with various ferromagnetic (FM) layers.[5–10)] However, the interfacial oxidation might be severe at elevated temperatures for the metallic FM layers.[11)] Furthermore, the electrical manipulation on the exchange bias in BFO-based bilayers has been demonstrated to be irreversible.[12–14)]

Half metallic manganite perovskite with very high spin polarization [at least 95% for $La_{0.67}Sr_{0.33}MnO_3$ (LSMO)[15)]] has been widely used as spin source in spintronics,[16)] and is the suitable oxide FM layer without structural deterioration of the interfacial oxidation, and has pseudo-cubic structure with similar lattice constant with BFO, providing the epitaxial growth of films. Clear exchange bias has been observed in $BFO/La_{0.7}Sr_{0.3}MnO_3$ bilayers with reversible electrical field controllable exchange bias.[17,18)] In spite of the high film quality by the epitaxial growth on (001) $SrTiO_3$ (STO) substrate, the blocking temperature of exchange bias is only about 100 K,[7,17)] which is much lower than the FM Curie temperature of $La_{0.7}Sr_{0.3}MnO_3$ ($T_{C\text{-}FM} \sim 350$ K)[19)] and T_N of BFO. Furthermore, the electrical manipulation of the exchange bias can only be observed below 30 K.[18)] Thus, it is important to understand the mechanism of the exchange bias in BFO/LSMO bilayers to extend the multiferroic operation temperature to RT. In this paper, we studied the exchange bias in (001) BFO/LSMO and (111) BFO/LSMO bilayers. Only coercivity enhancement has been observed in (111) BFO/LSMO bilayers, while both exchange bias field and coercivity enhancement have been observed in (001) BFO/LSMO bilayers. Our results demonstrate that there is possible interfacial spin glass at the ferroelectric domain walls of BFO which contributes to the exchange bias field, while the domains contribute to the coercivity enhancement.

2. Experimental methods

2.1 Films preparation

The LSMO and BFO layers were deposited on the single-crystal (001) and (111) STO substrates by pulsed laser deposition (PLD). During the deposition, the substrate temperature (T_s) was fixed to 850 °C with oxygen pressure (P_{O2}) of 30 Pa for the LSMO layers, 700 °C and 7 Pa for the BFO layers. The thickness of layers was controlled by the laser pulse number. For the exchange bias study, the structure of STO/LSMO (300 pulses, ~12 nm)/BFO (1000 pulses, ~80 nm) was selected. Single layer LSMO films of the same thickness were also deposited on (001) and (111) STO substrates under the same conditions as the bilayers for the comparative studies. Since the lattice constant of BFO (3.96 Å, pseudo-cubic) is larger than that of LSMO (3.873 Å),[20,21)] in-plane tensile strain might be induced in LSMO layer. For comparison, the BFO was replaced by $PbZr_{0.52}Ti_{0.48}O$ (PZT; $T_s = 800$ °C, $P_{O2} = 20$ Pa) with the same laser pulse number on (001) STO substrates to study the influence of tensile strain at top interface on the magnetic properties of LSMO, because the a lattice constant of PZT (4.036 Å, tetragonal; PDF No. 330784) is close to that of BFO.

2.2 Characterizations

The structure of the films was characterized by X-ray diffraction (XRD) with Cu Kα radiation. Temperature dependent magnetic properties were carefully measured by a commercial dc magnetometer (Quantum Design MPMS SQUID VSM) from 5 to 300 K. In order to obtain accurate values of H_E and H_C, care was taken to minimize the residual magnetic field to almost zero before measurements. The surface morphology and ferroelectric domains were characterized by scanning probe microscopy (SPM; Asylum Research Cypher). For simplicity, we use (001) to denote

 © 2014 The Japan Society of Applied Physics

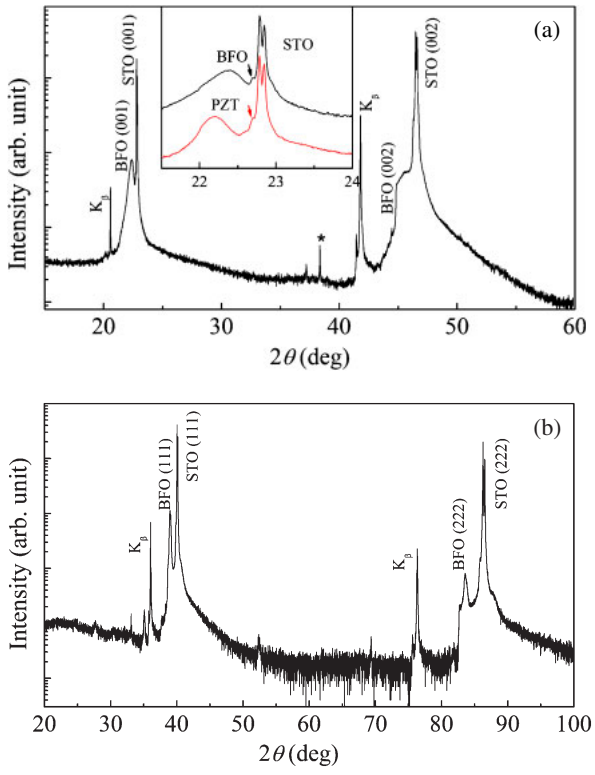

Fig. 1. (Color online) XRD patterns of (a) (001) BFO/LSMO and (b) (111) BFO/LSMO bilayers. The "∗" marks the diffraction peaks from STO substrate, and the diffraction due to K_β is also marked. The inset in (a) shows the enlarged view around the STO (001) peak for (001) BFO/LSMO and (001) PZT/LSMO bilayers.

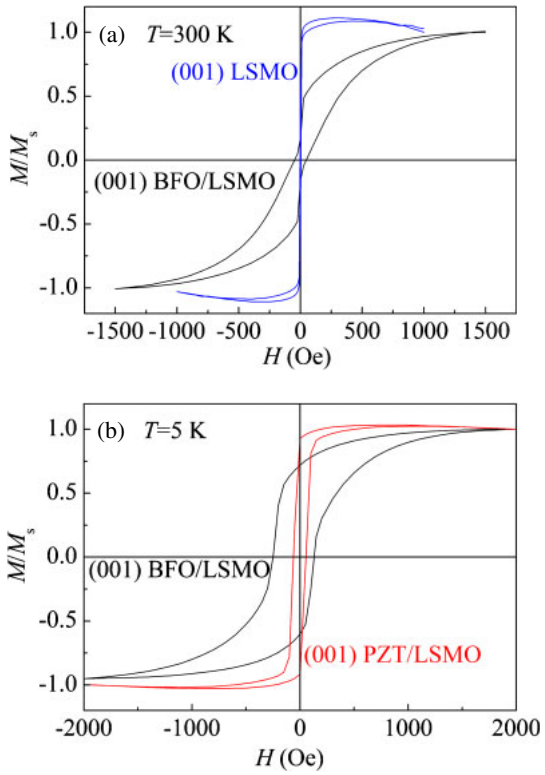

Fig. 2. (Color online) (a) *M–H* curves for (001) LSMO film and (001) BFO/LSMO bilayers measured at 300 K. (b) *M–H* curves for (001) BFO/LSMO and (001) PZT/LSMO bilayers measured at 5 K.

the films deposited on (001) STO substrates, while (111) to denote the films deposited on (111) STO substrates.

3. Results and discussion

Figure 1 shows the XRD patterns of (001) and (111) BFO/LSMO bilayers. All the peaks are indexed to the pseudo-cubic structure. Due to the epitaxial growth on the single crystalline (001) and (111) STO substrates, only (001) and (002) peaks of BFO on (001) STO substrates, and (111) and (222) peaks of BFO on (111) STO substrates, can be observed. The LSMO (001) and (002), (111) and (222) peaks cannot be resolved in the XRD patterns, which might be due to the close lattice constant between LSMO (3.873 Å) and STO (3.905 Å) in the pseudo-cubic structure.[21] The LSMO film is too thin, and the diffraction peaks are weak and overlapped by the diffraction peaks of STO. The inset of Fig. 1(a) shows the enlarged view around the STO (001) peak for (001) BFO/LSMO and (001) PZT/LSMO bilayers. The small diffraction peaks marked by arrows are from the STO substrates. The (001) peak of PZT locates at the left to that of BFO, for the larger *c* lattice constant of PZT than that of BFO.

The magnetic properties of (001) BFO/LSMO bilayers were first studied. The RT field dependent magnetization (*M–H*) loops for (001) LSMO and (001) PZT/LSMO are shown in Fig. 2(a). Double hysteresis loop can be observed for (001) BFO/LSMO. We attribute this to the different location of the LSMO layer on BFO, soft on the ferroelectric domain walls and hard on the ferroelectric domains of BFO, which will be discussed later. No significant shift of the loop can be observed, indicating the lacking of the exchange bias field (H_E) at RT. At 5 K, the H_E of 60 Oe can be clearly observed in (001) BFO/LSMO. Here, H_E is defined as $H_E = -(H_{C1} + H_{C2})/2$, where H_{C1} and H_{C2} are the left and right coercive fields, respectively. Recently Shi et al. reported the tensile strain on ultrathin LSMO film may induce AFM structure and provides exchange bias on the neighboring FM layer.[22] For comparison, H_E of only about 4 Oe can be observed for (001) PZT/LSMO which is close to the limitation of our measuring system. Thus the contribution on H_E from the possible in-plane tensile strain on the top surface of LSMO can be excluded.

The temperature dependent H_E and H_C are shown in Fig. 3. Compared to the almost zero H_E and gradually increasing H_C with decreasing T for (001) PZT/LSMO, clear H_E and significantly enhanced H_C for (001) BFO/LSMO can both be observed below 150 K after cooling in field of 2000 Oe. Safeer et al. has suggested the low temperature exchange coupling from the spin glass in BFO.[23] Generally, the net spins in 109° domain walls in $BiFeO_3$ have been considered to be the main origin of the exchange bias.[24,25] Due to the complicated exchange interaction at the interface,[7] e.g., AFM for Fe^{3+}–O^{2-}–Fe^{3+} and FM for Fe^{3+}–O^{2-}–Mn^{3+} and Fe^{3+}–O^{2}–Mn^{4+}, spin glass might be formed at domain walls in BFO at the interface, and the exchange bias might originate from the exchange coupling between LSMO and the spin glass, which has also been confirmed by our recent study on the exchange bias in BFO/NiFe and BFO/Co bilayers.[26] The formation of the spin glass is confirmed by the asymmetry along the *M* axis for each *M–H* loop of (001) BFO/LSMO, which is represented by ΔM and its temper-

© 2014 The Japan Society of Applied Physics

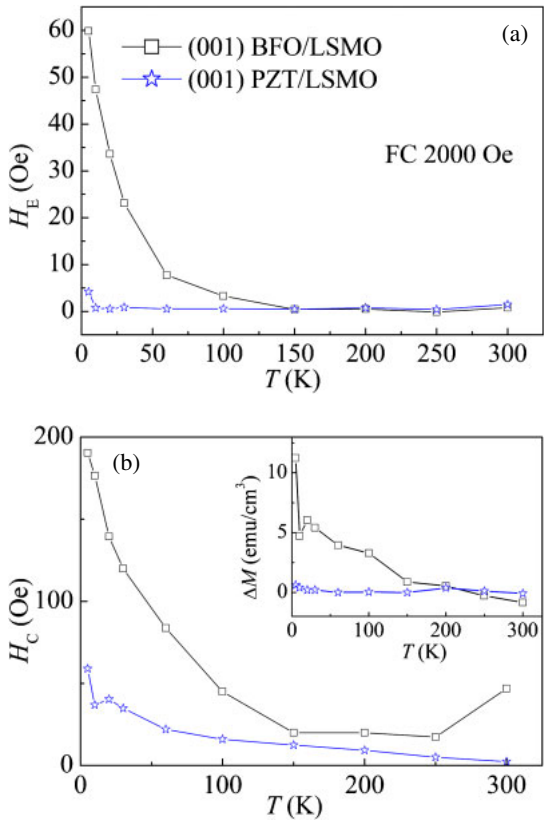

Fig. 3. (Color online) (a) H_E–T and (b) H_C–T curves for (001) BFO/LSMO and (001) PZT/LSMO bilayers. The inset shows the ΔM–T curves for (001) BFO/LSMO and (001) PZT/LSMO bilayers.

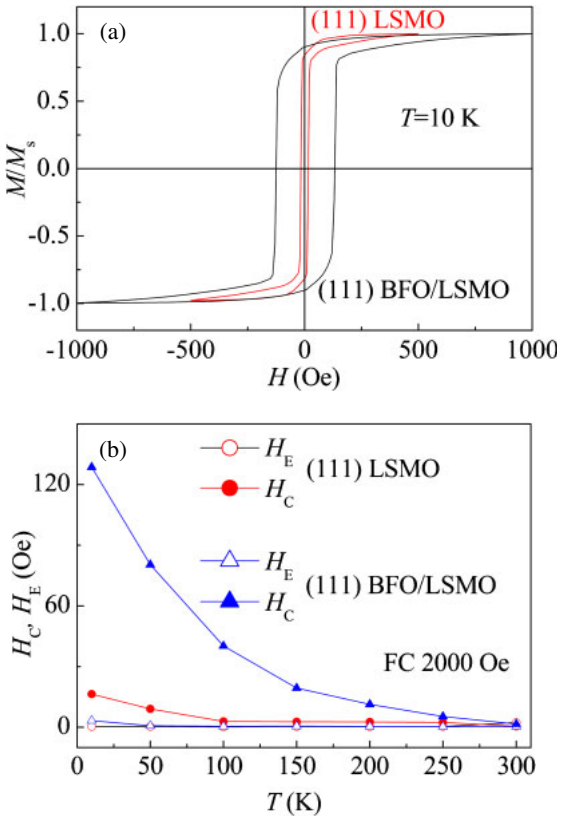

Fig. 4. (Color online) (a) M–H curves for (111) LSMO film and (111) BFO/LSMO bilayers measured at 10 K (b) the temperature dependent H_E and H_C for (111) LSMO film and (111) BFO/LSMO bilayers.

ature dependence in the inset of Fig. 3(b). Here, ΔM means half of the difference between the magnetic moments at positive and negative saturation states. For comparison, nearly zero ΔM was observed for (001) PZT/LSMO, since no exchange coupling between PZT and LSMO. The ΔM increases significantly when T is below 150 K, suggesting the interfacial frustrated spins frozen and aligned to the cooling field direction. Because this variation behavior of ΔM is much similar to that of H_E at the same temperature range, it is reasonable to infer that they come from the same origin, i.e., the interfacial spin glass. If we take the ~0.6 μ_B/Fe[7] and the area fraction of the domain walls of 2%,[24] the FM contribution from a pseudo-cubic unit cell of BFO at domain walls is about 5.8 emu/cm^3, which is quite reasonably consistent with the measured magnetization from the spin glass. This further confirms the location of spin glass in the domain walls of BFO at interface. The positive vertical magnetization of the M–H curve for (001) BFO/LSMO bilayers suggests the interfacial FM coupling,[27] which is due to the FM superexchange coupling between Fe^{3+} and Mn^{3+}, and Fe^{3+} and Mn^{4+}.[7] With the field cooling, the magnetization of the spin glass will be forced to be pinned and parallel to the field direction due the FM coupling with the LSMO layer, leading to the negative H_E and positive ΔM.

To further confirm the contribution of domains and domain walls on the exchange bias, we studied the exchange bias effect in the (111) BFO/LSMO bilayers. As shown in Fig. 4(a), significantly enhanced coercivity compared with the (111) LSMO film can be observed at 10 K. However, no significant shift along the field and magnetization of the M–H curve can be observed. The H_E is only about 3 Oe, which is much smaller than that in the (001) BFO/LSMO bilayers. Furthermore, the ΔM for the M–H curve of (111) BFO/LSMO bilayers is only about 0.7 emu/em^3, which is almost one order smaller than that of the (001) BFO/LSMO bilayers. Figure 4(b) shows the temperature dependent H_E and H_C for (111) BFO/LSMO bilayers. No significant H_E in the measuring temperature range between 10 and 300 K can be observed, while the enhancement of the H_C can be observed up to 300 K.

As the interface roughness might influence the exchange bias in the AFM/FM bilayers, we investigated the surface roughness of (001) and (111) LSMO layer by atomic force microscopy, and the images are shown in Fig. 5(a). As can be clearly seen, both films are very smooth. The measured surface roughness (rms value) of (001) LSMO is 0.24 nm, while that of the (111) LSMO is 0.1 nm. Thus, the influence of surface roughness on the exchange bias can be excluded. As there are four possibilities in the in-plane projection of the polarization, the in-plane domain patterns of both (001) BFO and (111) BFO films were studied by the piezoelectric force microscopy (PFM), and are shown in Figs. 5(c) and 5(d), respectively. The domain size of the (001) BFO is about several tens of nm, while the domain size of (111) BFO film is about several μm. Chu et al. have reported the single-domain state in the (111) BFO film.[28] It should be noted that the STO substrates in our studies were prepared by the floating zone method, thus there might be mosaic structure with grains of large size. The ⟨111⟩ polarization of the BFO film might slightly tilt from the normal of the film surface due

© 2014 The Japan Society of Applied Physics

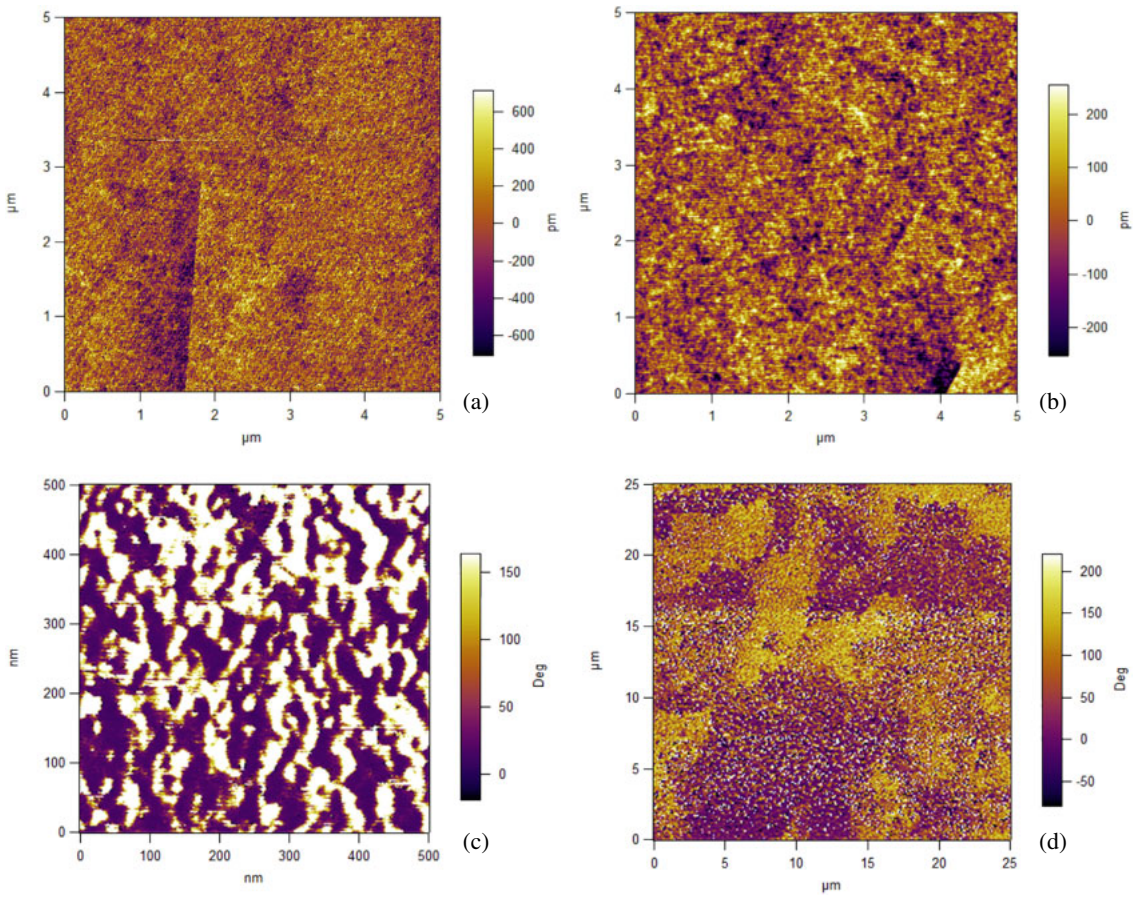

Fig. 5. (Color online) AFM images for (a) (001) LSMO and (b) (111) LSMO films In-plane PFM images for (c) (001) BFO and (d) (111) BFO films.

to the epitaxial growth on different grains of the substrates, leading to the smaller in-plane component of the polarization. However, the domain size of the (111) BFO is about 2 orders larger than that of the (001) BFO, suggesting the negligible domain walls in the (111) BFO films. Thus we can further conclude that the exchange bias field with blocking temperature of about 150 K in (001) BFO/LSMO bilayers originates from the high density of domain walls, while the domains contribute to the coercivity enhancement. Above 150 K, the spins cannot be blocked, so the magnetization of LSMO cannot be pinned, leading to the disappearance of the H_C enhancement and H_E. The exchange coupling with domains can persist up to RT, leading to the H_C enhancement. In (001) BFO/LSMO bilayers, there is high density of domain walls in BFO, LSMO layer will exhibit soft magnetic properties on the domain walls of BFO while hard magnetic properties on the domains of BFO, leading to the observation of the double hysteresis loop.

It should be noted that the exchange bias on (001) BFO and (111) BFO is not restricted on LSMO, exchange bias field has been observed in (001) BFO/CoFe but only coercivity enhancement in (111) BFO/CoFe.[29] We have also got the similar results on BFO/NiFe bilayers. Lebeugle et al. suggested that the exchange coupling between the FM layer and the BFO is related to the net spins in BFO due to the spin canting in the cycloidal modulated AFM structure.[30] The exchange coupling should induce a wriggling of the FM magnetization along the underlying cycloid in BFO. However, for a given polarization, there are three possible cycloidal directions, leading to the three possible pinned FM magnetization directions. Thus, only coercivity enhancement without exchange bias field can be observed, though there is interface exchange coupling between the LSMO and BFO domains. Due to the much lower temperature of the spin glass induced exchange bias, the domain contribution to the exchange bias should be utilized for the daily multiferroic applications. A better control of the cycloidal direction might be essential for inducing exchange bias field through the exchange coupling with the BFO domains, and the electrical manipulation of the pinned FM magnetization via the magnetoelectric coupling.

4. Conclusions

In conclusion, BFO/LSMO bilayers were deposited on the (001) and (111) STO substrates by PLD, and the exchange bias effect in the bilayers has been systematically studied. Clear H_E with blocking temperature of about 150 K and enhanced coercivity at room temperature has been observed in (001) BFO/LSMO bilayers, while only enhanced coercivity without H_E down to 10 K has been observed in (111) BFO/LSMO bilayers. By the comparative study on the (001) PZT/LSMO bilayer, the contribution of the interface tensile strain on the exchange bias effect has been excluded. The blocking temperature of H_E in (001) BFO/LSMO bilayers coincides well with the emerging temperature of the vertical magnetization shift due to the blocking of the interfacial spin glass. The PFM images show that the domain size of (111) BFO is 2 orders larger than that of the (001)

© 2014 The Japan Society of Applied Physics

BFO, indicating the much higher domain wall density in (001) BFO. Our results clearly demonstrate that the exchange coupling with the interfacial spin glass at the domain walls in BFO contributes to the H_E with blocking temperature of about 150 K, while the exchange coupling with the domains contributes to the enhanced coercivity up to room temperature. Our results suggest that for the RT multiferroic application of BFO, the exchange coupling with the BFO domains should be utilized and a better control of the spin cycloidal modulation direction is required.

Acknowledgements

This work is supported by the National Key Projects for Basic Researches of China (2010CB923401 and 2010CB923404), the National Natural Science Foundation of China (51172044, 11074112, 11174131), the National Science Foundation of Jiangsu Province of China (BK2011617), and the Scientific Research Foundation for the Returned Overseas Chinese Scholars, State Education Ministry.

1) R. Ramesh, Nat. Mater. **9**, 380 (2010).
2) G. Catalan and J. F. Scott, Adv. Mater. **21**, 2463 (2009).
3) T. Zhao, A. Scholl, F. Zavaliche, K. Lee, M. Barry, A. Doran, M. P. Cruz, Y. H. Chu, C. Ederer, N. A. Spaldin, R. R. Das, D. M. Kim, S. H. Baek, C. B. Eom, and R. Ramesh, Nat. Mater. **5**, 823 (2006).
4) M. Bibes and A. Barthélémy, Nat. Mater. **7**, 425 (2008).
5) J. Dho and M. G. Blamire, J. Appl. Phys. **106**, 073914 (2009).
6) J. Allibe, I. C. Infante, S. Fusil, K. Bouzehouane, E. Jacquet, C. Deranlot, M. Bibes, and A. Barthélémy, Appl. Phys. Lett. **95**, 182503 (2009).
7) P. Yu, J. S. Lee, S. Okamoto, M. D. Rossell, M. Huijben, C. H. Yang, Q. He, J. H. Zhang, S. Y. Yang, M. J. Lee, Q. M. Ramasse, R. Erni, Y. H. Chu, D. A. Arena, C. C. Kao, L. W. Martin, and R. Ramesh, Phys. Rev. Lett. **105**, 027201 (2010).
8) T. L. Qu, Y. G. Zhao, P. Yu, H. C. Zhao, S. Zhang, and L. F. Yang, Appl. Phys. Lett. **100**, 242410 (2012).
9) H. Béa, M. Bibes, S. Cherifi, F. Nolting, B. Warot-Fonrose, S. Fusil, G. Herranz, C. Deranlot, E. Jacquet, K. Bouzehouane, and A. E. Barthélémy, Appl. Phys. Lett. **89**, 242114 (2006).
10) T. Hauguel, S. P. Pogossian, D. T. Dekadjevi, D. Spenato, J. Jay, M. V. Indenbom, and J. B. Youssef, J. Appl. Phys. **110**, 073906 (2011).
11) H. Naganuma, M. Oogane, and Y. Ando, J. Appl. Phys. **109**, 07D736 (2011).
12) J. Allibe, S. Fusil, K. Bouzehouane, C. Daumont, D. Sando, E. Jacquet, C. Deranlot, M. Bibes, and A. Barthélémy, Nano Lett. **12**, 1141 (2012).
13) E. Choi, E. Weal, Z. Bi, H. Wang, A. Kursumovic, T. Fix, M. G. Blamire, and J. L. MacManus-Driscoll, Appl. Phys. Lett. **102**, 012905 (2013).
14) W. Ratcliff, II, Z. Yamani, V. Anbusathaiah, T. R. Gao, P. A. Kienzle, H. Cao, and I. Takeuchi, Phys. Rev. B **87**, 140405 (2013).
15) M. Bowen, M. Bibes, A. Barthélémy, J.-P. Contour, A. Anane, Y. Lemaître, and A. Fert, Appl. Phys. Lett. **82**, 233 (2003).
16) I. J. Vera Marún, F. M. Postma, J. C. Lodder, and R. Jansen, Phys. Rev. B **76**, 064426 (2007).
17) S. M. Wu, S. A. Cybart, P. Yu, M. D. Rossell, J. X. Zhang, R. Ramesh, and R. C. Dynes, Nat. Mater. **9**, 756 (2010).
18) S. M. Wu, S. A. Cyart, D. Yi, J. M. Parker, R. Ramesh, and R. C. Dynes, Phys. Rev. Lett. **110**, 067202 (2013).
19) M. Belmeguenai, S. Mercone, C. Adamo, P. Moch, D. G. Schlom, and P. Monod, J. Appl. Phys. **109**, 07C120 (2011).
20) Y. Liu, Y. Yao, S. Dong, S. Yang, and X. Li, Phys. Rev. B **86**, 075113 (2012).
21) D. Gutiérrez, M. Foerster, I. Fina, J. Fontcuberta, D. Fritsch, and C. Ederer, Phys. Rev. B **86**, 125309 (2012).
22) Y. J. Shi, Y. Zhou, H. F. Ding, F. M. Zhang, L. Pi, Y. H. Zhang, and D. Wu, Appl. Phys. Lett. **101**, 122409 (2012).
23) C. K. Safeer, M. Chamfrault, J. Allibe, C. Carretero, C. Deranlot, E. Jacquet, J.-F. Jacquot, M. Bibes, A. Barthélémy, B. Dieny, H. Béa, and V. Baltz, Appl. Phys. Lett. **100**, 072402 (2012).
24) L. W. Martin, Y. Chu, M. B. Holcomb, M. Huijben, P. Yu, S. Han, D. Lee, S. X. Wang, and R. Ramesh, Nano Lett. **8**, 2050 (2008).
25) H. Béa, M. Bibes, F. Ott, B. Dupé, X.-H. Zhu, S. Petit, S. Fusil, C. Deranlot, K. Bouzehouane, and A. Barthélémy, Phys. Rev. Lett. **100**, 017204 (2008).
26) X. B. Xue, X. Y. Yuan, W. B. Rui, Q. Y. Xu, B. You, W. Zhang, S. M. Zhou, and J. Du, Eur. Phys. J. B **86**, 121 (2013).
27) W. Zhang, T. Wen, and K. M. Krishnan, Appl. Phys. Lett. **101**, 132401 (2012).
28) Y. Chu, M. P. Cruz, C. Yang, L. W. Martin, P. Yang, J. Zhang, K. Lee, P. Yu, L. Chen, and R. Ramesh, Adv. Mater. **19**, 2662 (2007).
29) F. Bai, G. Yu, Y. Wang, L. Jin, H. Zeng, X. Tang, Z. Zhong, and H. Zhang, Appl. Phys. Lett. **101**, 092401 (2012).
30) D. Lebeugle, A. Mougin, M. Viret, D. Colson, and L. Ranno, Phys. Rev. Lett. **103**, 257601 (2009).

© 2014 The Japan Society of Applied Physics